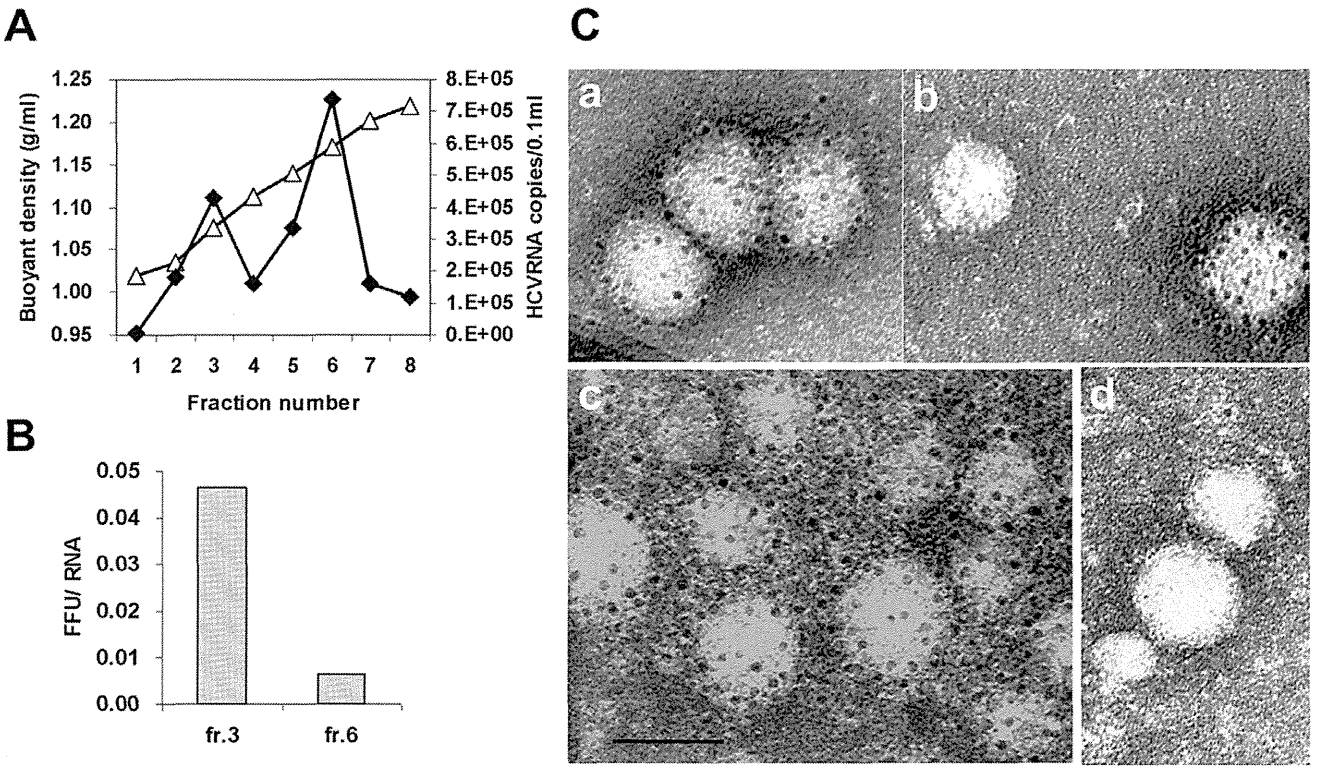

Figure 5. Immuno-gold EM demonstrated that both #37 and #55 recognized HCV intact particles. (**A**). Equilibrium SDG centrifugation. ◆, HCV RNA copies measured by RT-qPCR; Δ, buoyant densities. (**B**). The ratio of infectivity titer (FFU) to HCV RNA copies of fractions 3 and 6. (**C**). Immuno-gold EM. Viral particles in fraction 3 were treated with #37 (**a, b**), #55 (**c**), or a control antibody (**d**) followed by anti-human IgG conjugated with colloidal gold particles, and examined under an electron microscope. HCV-like particles in the sample treated with #37 and #55 were observed with specific labeling of gold particles indicating that the antibodies are capable of binding to viral particles. Bar = 50 nm.
doi:10.1371/journal.pone.0055874.g005

HCV were tested in the assays. The one virus-sample contained 10^2 FFU/0.1 ml (no.1) and another 10^3 FFU/0.1 ml (no.2). **Table 2** shows the 50% neutralization titers (NT_{50}) of #55, a lowest concentration (μg/ml) required for 50% reduction of FFU, calculated by curvilinear regression analysis. #55 neutralized HCV infection of various genotypes (1a, 1b, 2a, 3a, 4a, 5a, and 6a), with the NT_{50} titers ranging from 2 to 127 μg/ml for no.1 and 6 to 231 μg/ml for no.2. Neutralization of genotype 7a (QC69/JFH1) by #55 was less, with a NT_{50} titer of 219 μg/ml for no.1 and >500 μg/ml for no.2.

Blocking of Viral Adsorption

We examined whether #55 blocked viral adsorption to cells by measuring the amount of cell-attached HCV RNA using RT-qPCR. A half ml of the culture supernatant containing 10^5 FFU/ml of chimeric HCV, H77/C3, was pre-treated at 4°C for 24 h with an equal volume of #55, #37 or a control antibody at a final

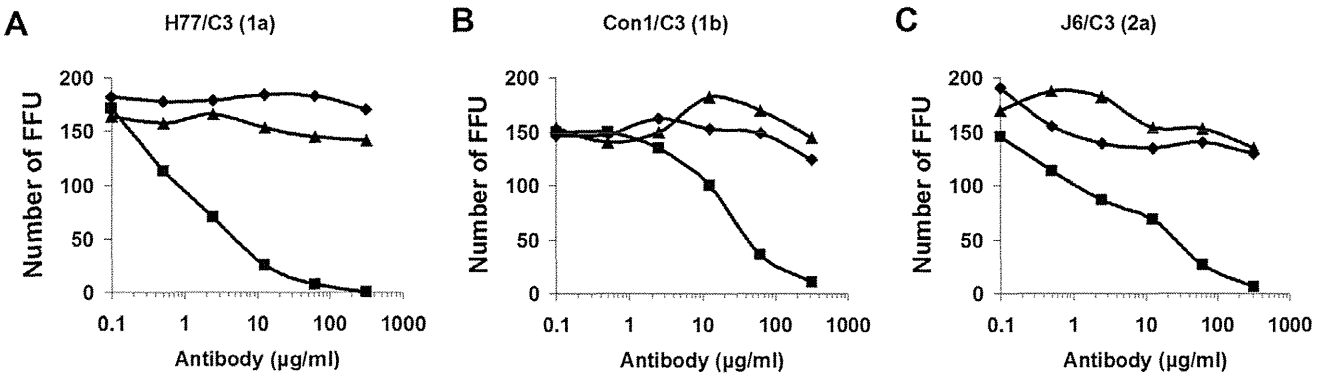

Figure 6. Neutralization assay by FFU reduction. The mean numbers of positive foci are shown for viruses H77/C3 (**A**), Con1/C3 (**B**), and J6/C3 (**C**). Compared to the results obtained with an irrelevant control antibody, #55 inhibited the viral infection in dose-dependent manner for all of the 3 samples tested. Inhibition by #37 was not observed. ◆, control; ■, #55; ▲, #37.
doi:10.1371/journal.pone.0055874.g006

Table 2. 50% neutralization titers (NT_{50}) of #55 by FFU reduction.

Virus (genotype)	NT_{50} (μg/ml)*	
	no.1	no.2
H77C/JFH1 (1a)	10.6	10.3
J4/JFH1 (1b)	ND	9.3
J6/JFH1 (2a)	126.6	99.1
J8/JFH1 (2b)	21.1	24.1
S52/JFH1 (3a)	73.0	230.8
ED43/JFH1 (4a)	1.3	7.4
SA13/JFH1 (5a)	5.0	5.7
HK6a/JFH1 (6a)	5.2	7.3
QC69/JFH1 (7a)	218.5	>500
JFH1 (2a)	2.0	ND

*, calculated by curvilinear regression analysis; ND, not done.
doi:10.1371/journal.pone.0055874.t002

concentration of 500, 50, or 5 μg/ml. The mixtures were then inoculated onto Huh7.5 cells seeded in 12-well plates (5×10^5 cells/well). After incubation for 4 h at 37°C, cells were washed 3 times with PBS. Amount of cell-associated HCV RNA in a well was measured by RT-qPCR. Each test was performed in duplicate. Compared to the control antibody (human IgG), #55 inhibited viral adsorption in dose-dependent manner, as shown in **Figure 7**. Inhibition by #37 was not observed but rather slightly enhanced at a concentration of 50 μg/ml.

Specific amino acids (W420, Y527, W529, G530, and D535) in the E2 envelope protein of HCV were reported to be critical for binding to CD81, a principal cellular receptor and they were conserved across all genotypes [26]. As the epitope of #55 includes these amino acid residues, it was possible that #55 blocked virus adsorption by competing with CD81 for a binding site on the E2 envelope. **Figure 8A** shows sequence alignment of aa 508 to 607, the epitope of #55, of HCV employed in the present study. The epitope of #55 contains the residues important for binding to CD81 (asterisks). Thus, we investigated this possibility by testing whether CD81 inhibits binding of HCV to #55 utilizing an assay based on antibody-captured RT-qPCR. A

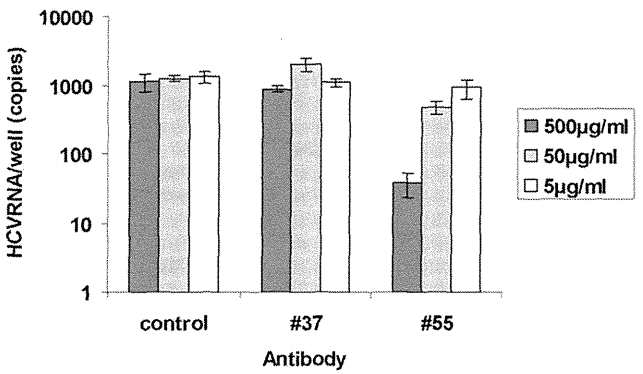

Figure 7. Blocking of viral adsorption by #55. Blocking of viral adsorption measured by RT-qPCR. Compared to the control antibody (human IgG), #55 inhibited viral adsorption in dose-dependent manner. Inhibition by #37 was not observed but rather slightly enhanced at a concentration of 50 μg/ml.
doi:10.1371/journal.pone.0055874.g007

100 μl of the virus solution containing 10^4 FFU/ml of H77/C3 was incubated with an equal volume of various dilutions of soluble recombinant human CD81 protein (Origene, Rockville, MD, USA) for 2 h at room temperature. Each mixture was then inoculated into a 48-well plate which was pre-coated with #55 or an irrelevant control antibody (human IgG) at a concentration of 10 μg/ml. The plate was incubated at 4°C overnight. After washing, bound HCV RNA was extracted and quantified by RT-qPCR. As shown in **Figure 8B**, CD81 inhibited the binding of virus to #55 in a dose-dependent manner.

Discussion

In this study, as an approach to obtain human B cell lines producing antibodies to HCV envelope E2, we applied the EBV transformation method, which is based on the fact that EBV transforms B-lymphocytes of humans *in vitro* into lymphoblastoid cells that synthesize and secrete immunoglobulins. From PBMC collected from a patient persistently infected with HCV strain H (genotype 1a) we have successfully isolated two clones producing anti-HCV E2 antibodies, #37 and #55. At the first screening of culture supernatants, several wells of a 96-well plate were found positive for anti-HCV E2 antibodies. However, most of them became negative as further cultured. Finally #37 and #55 remained as stably producing clones.

There was remarkable contrast between these two antibodies in their properties: (1) #55 appeared to be a broadly cross-neutralizing antibody. In the neutralization assay by FFU reduction, it inhibited infection by HCV genotypes 1a, 1b, 2a, 2b, 3a, 4a, 5a, 6a, and, to a lesser extent, 7a. In contrast, #37 did not neutralize any of the viruses tested. Interestingly it tended to enhance the infection at low concentrations (**Figure 6B and C,** and **Figure 7**): (2) the epitope of #55 was mapped to the region of aa 508 to 607 and that of #37 was mapped to the longer region spanning aa 429 to 652 of the E2 protein. #55 seemed unique for broadly cross-neutralizing antibody to have a relatively short conformational epitope, since it has been reported that conformational epitopes reacting with such antibodies are usually retained in the full length E2 [7,9]: (3) when we tested their cross-reactivity using transfected Huh7 cells expressing the E2 proteins, #37 was reactive with genotype 1a but reacted very weakly with the others, while #55 was broadly reactive with all genotypes tested. However, when examined using the virus-infected cells as targets, #37 was reactive with all HCV genotypes tested, although its binding activity measured by IF was less than that of #55 except for H77C/JFH1(1a) and S52/JFH(3a): (4) in immuno-gold EM, viral particles recognized by #37 were rather homogenous in size and measured approximately 50–60 nm in diameter. On the other hand, #55 produced larger aggregates of various-sized viral particles, probably because of its higher binding activity: (5) the antibodies showed a different pattern of IF-staining in the HCV-infected cells. While #37 gave granular reactions mostly in the periphery of nuclei, #55 gave diffuse staining throughout the cytoplasm (**Figure 4**). The nature of the antigens reacting with #37 and #55 remains to be studied.

Recently, Keck et al. reported that the region aa 529 to 535 of the E2 envelope protein is a CD81 binding region that does not tolerate neutralization escape mutations [27]. The epitope of #55 includes the above mentioned region and #55 blocked virus adsorption by competing with CD 81 for a binding site on the E2 envelope. As #55 is broadly neutralization cross-reactive, it may be very useful in preventing infection by HCV of various genotypes. Sasayama et al. reported that blocking N-glycosylation of aa 534 (aa 532 of strain H77) in this region by substituting

A

```
                   508          • • • ••   •                552                                                      607   References
H77/C3(1a)         CFTPSPVVVGTTDRSGAPTYSWGANDTDVFVLNNTRPPLGNWFGCTWMNSTGFTKVCGAPPCVI.GGVGNNT....LLCPTDCFPKHPEATYSRCGSGPWITPRC   [17]
Con1/C3(1b)        --------------F-V------E-E---LL-------Q----------------T--G---N-.--I--K-....-T------R-------TK------L----   [17]
J6/C3(2a)          --------------L-----T--E-E----L--S------S---------------T------RT.RADFNASTD..---------R---DT--LK------L----   [17]
JFH1(2a)           --------------R-V---T--E-E----L--S----Q-S---------S-Y--T------RT.RADFNASTD..---------R---D---IK------L--K-   [5]
H77C/JFH1(1a)      ----------------------------------------------------------------.-------....---------R--------------------   [20]
J4/JFH1(1b)        ----------------V------E-E---ML-------Q----------------T--G---N-.-----R-....-I------R-------TK------L----   [18]
J6/JFH1(2a)        --------------L-----T--E-E----L--S------S---------S-Y--T------RT.RADFNASTD..---------R---DT--LK------L----   [19]
J8/JFH1(2b)        -------------KQ-V---T--E-E----L--S----R-A--------G-----T------R-.RKDY-S-ID..---------R---D---LK--A---L----   [18]
S52/JFH1(3a)       -------------IK-K---N--E-E----L-ESL---S-R----A-------L-T------N-Y--E-DPENETD-F------R-----------A---L----   [22]
ED43/JFH1(4a)      -------------HV-V---T--E-E----L--S----H-A----V---------T------EV.NTNNGT.....WH------R----T--AK-----------   [20]
SA13/JFH1(5a)      --------------K-N------E-E--I-L-------T-------------V-T------NL.-PT---S.....K------R---D---TK------L----   [21]
HK6a/JFH1(6a)      -------------KL-I---N--E-E----M-ESL---T-G-------------T------Q-.VPGDY-SSANE--------R-------Q-----------   [18]
QC69/JFH1(7a)      --------------R-V---T--E-ES---L--S----Q-S----S---T-----T--G---K-.RPQ-AQSNTS.-T------R---R----A------L----   [18]
```

☆, important amino acids for binding to CD81[26]

B

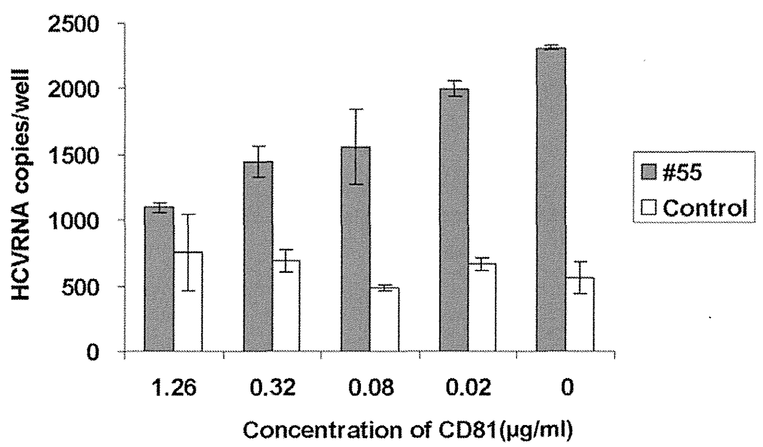

Figure 8. Binding of HCV to #55 was inhibited by soluble recombinant CD81. (**A**). Sequence alignment of aa 508 to 607, the epitope of #55, of various genotypes of HCV employed in the present study. Residues identical to the sequences of H77/C3 are indicated by a dash. Dots indicate gaps. (**B**). H77/C3 virus was treated with various dilutions of soluble CD81.The mixtures were inoculated into a 48-well plate that was pre-coated with #55 or the control antibody. Amount of bound HCV RNA was measured by RT-qPCR.
doi:10.1371/journal.pone.0055874.g008

asparagine with histidine markedly enhanced the sensitivity of the virus to neutralizing antibodies and suggested that the aa 529 to 535 region is usually protected from the antibody's access by the N-glycosylation [28]. It is possible that #55 may evade the N-glycosylation mediated protective mechanism of HCV.

A cross-neutralizing monoclonal antibody that could be generated in large volume might be particularly beneficial to prevent the almost universal occurrence of HCV re-infection of transplanted livers and could play other roles in immunoprophylaxis until such time as an effective HCV vaccine is developed and commercialized.

Acknowledgments

We thank Mari Komoto (Kobe University, Kobe, Japan) for technical assistance.

Author Contributions

Conceived and designed the experiments: YKS RHP. Performed the experiments: YKS MH MO. Analyzed the data: YKS KS HY HH. Contributed reagents/materials/analysis tools: HJA. Wrote the paper: YKS RHP HJA HY.

References

1. Shimizu YK, Hijikata M, Iwamoto A, Alter HJ, Purcell RH, et al. (1994) Neutralizing antibodies against hepatitis C virus and the emergence of neutralization escape mutant viruses. J Virol 68: 1494–1500.
2. Logvinoff C, Major ME, Oldash D, Heyward S, Talal A, et al. (2004) Neutralizing antibody response during acute and chronic hepatitis C virus infection. Proc Natl Acad Sci U S A 101: 10149–10154.
3. Ishii K, Rosa D, Watanabe Y, Katayama T, Harada H, et al. (1998) High titers of antibodies inhibiting the binding of envelope to human cells correlate with natural resolution of chronic hepatitis C. Hepatology 28: 1117–1120.
4. Farci P, Alter HJ, Wong DC, Miller RH, Govindarajan S, et al. (1996) Prevention of hepatitis C virus infection in chimpanzees by hyperimmune serum against the hypervariable region 1 of the envelope 2 protein. Proc Natl Acad Sci U S A 93: 15394–15399.
5. Wakita T, Pietschmann T, Kato T, Date T, Miyamoto M, et al. (2005) Production of infectious hepatitis C virus in tissue culture from a cloned viral genome. Nat Med 11: 791–796.
6. Meunier JC, Russell RS, Goossens V, Priem S, Walter H, et al. (2008) Isolation and characterization of broadly neutralizing human monoclonal antibodies to the E1 glycoprotein of hepatitis C virus. J Virol 82: 966–973.
7. Perotti M, Mancini N, Diotti RA, Tarr AW, Ball JK, et al. (2008) Identification of a broadly cross reacting and neutralizing human monoclonal antibody directed against the hepatitis C virus E2 protein. J Virol 82: 1047–1052.
8. Owsianka AM, Tarr AW, Keck ZY, Li TK, Witteveldt J, et al. (2008) Broadly neutralizing human monoclonal antibodies to the hepatitis C virus E2 glycoprotein. J Gen Virol 89: 653–659.

9. Mancini N, Diotti BA, Perotti M, Sautto G, Clementi N, et al. (2009) Hepatitis C virus (HCV) infection may elicit neutralizing antibodies targeting epitopes conserved in all viral genotypes. PLoS ONS 4: 1–7.
10. Broering TJ, Garrity KA, Boatright NK, Sloan SE, Sandor F, et al. (2009) Identification and Characterization of broadly neutralizing human monoclonal antibodies directed against the E2 envelope glycoprotein of hepatitis C virus. J Virol 83: 12473–12482.
11. Giang E, Dorner M, Prentoe JC, Dreux M, Evans MJ, et al. (2012) Human broadly neutralizing antibodies to the envelope glycoprotein complex of hepatitis C virus. Proc Natl Acad Sci U S A 109: 6205–6210.
12. Feinstone SM, Alter HJ, Dienes P, Shimizu Y, Popper H, et al. (1981) Non-A, non-B hepatitis in chimpanzees and marmosets. J Infect Dis 144: 588–597.
13. Blight KJ, Mckeating JA, Rice CM (2002) Highly permissive cell lines for subgenomic and genomic hepatitis C virus. J Virol 76: 13001–13014.
14. Shimizu YK, Purcell RH, Yoshikura H (1993) Correlation between the infectivity of hepatitis C virus in vivo and its infectivity in vitro. Proc Natl Acad Sci U S A 90: 6037–6041.
15. Shimizu YK, Hijikata M, Oshima M, Shimizu K, Yoshikura H (2006) Detection of a 5′ end subgenome of hepatitis C virus terminating at nucleotide 384 in patients' plasma and liver tissues. J Viral Hepatitis 13: 746–755.
16. Forns X, Allander T, Rohwer-Nutter P, Bukh J (2000) Characterization of modified hepatitis C virus E2 proteins expressed on the cell surface. Virology 274: 75–85.
17. Pietschmann T, Kaul A, Koutsoudakis G, Shavinskaya A, Kallis AS, et al. (2006) Construction and characterization of infectious intragenotypic and intergenotypic hepatitis C chimeras. Proc Natl Acad Sci U S A 103: 7408–7413.
18. Gottwein JM, Scheel TK, Jensen TB, Lademann JB, Prentoe JC, et al. (2009) Development and characterization of hepatitis C virus genotype 1–7 cell culture systems: role of CD81 and Scavenger Receptor Class B type 1 and effect of antiviral drugs. Hepatology 49: 364–377.
19. Yi-Ping L, Gottwein JM, Scheel TK, Jensen TB, Bukh J (2011) MicroRNA-122 antagonism against hepatitis C virus genotypes1–6 and reduced efficacy by host RNA insertion or mutations in the HCV 5′ UTR. Proc Natl Acad Sci U S A 108: 4991–4996.
20. Scheel TK, Gottwein JM, Jensen TB, Prentoe JC, Hoegh AM, et al. (2008) Development of JFH1-based cell culture systems for hepatitis C virus genotype 4a and evidence for cross-genotype neutralization. Proc Natl Acad Sci U S A 105: 997–1002.
21. Jensen TB, Gottwein JM, Scheel TK, Hoegh AM, Eugen-Olsen J, et al. (2008) Highly efficient JFH1-based cell culture system for hepatitis C virus genotype 5a: Failure of homologous neutralization-antibody treatment to control infection. J Infect Dis 198: 1756–1765.
22. Gottwein JM, Scheel TK, Hoegh AM, Lademann JB, Eugen-Olsen J, et al. (2007) Robust hepatitis C genotype 3a cell culture releasing adapted intergenotypic 3a/2a (S52/JFH1) viruses. Gastroenterology 133: 1614–1624.
23. Shimizu YK, Oomura M, Abe K, Uno M, Yamada E, et al. (1985) Production of antibody associated with non-A, non-B hepatitis in a chimpanzee lymphoblastoid cell line established by in vitro transformation with Epstein-Barr virus. Proc Natl Acad Sci U S A 82: 2138–2142.
24. Gastaminza P, Dryden K, Boyd B, Wood M, Law M, et al. (2010) Ultrastructural and biophysical characterization of hepatitis C virus particles produced in cell culture. J Virol 84: 10999–11009.
25. Hijikata M, Shimizu YK, Kato H, Iwamoto A, Shih JW, et al. (1993) Equilibrium centrifugation studies of hepatitis C virus: Evidence for circulating immune complexes. J Virol 67: 1953–1958.
26. Owsianka AM, Timms JM, Tarr AW, Brown JP, Hickling TP, et al. (2006) Identification of conserved residues in the E2 glycoprotein of the hepatitis C virus that are critical for CD81 binding. J Virol 80: 8695–8704.
27. Keck ZY, Saha A, Xia J, Wang Y, Lau P, et al. (2011) Mapping a region of hepatitis C virus E2 that is responsible for escape from neutralizing antibodies and a core CD81-binding region that does not tolerate neutralization escape mutations. J Virol 85: 10451–10463.
28. Sasayama M, Shoji I, Adianti M, Jiang DP, Deng L, et al. (2012) A point mutation at asn-534 that disrupts a conserved N-glycosylation motif of the E2 glycoprotein of hepatitis C virus markedly enhances the sensitivity to antibody neutralization. J Med Virol 84: 229–234.

HEPATOLOGY
Official Journal of the American Association for the Study of Liver Diseases

Free Cholesterol Accumulation in Hepatic Stellate Cells: Mechanism of Liver Fibrosis Aggravation in Nonalcoholic Steatohepatitis in Mice

Kengo Tomita,[1,2]* Toshiaki Teratani,[2]* Takahiro Suzuki,[2] Motonori Shimizu,[1] Hirokazu Sato,[1] Kazuyuki Narimatsu,[1] Yoshikiyo Okada,[1] Chie Kurihara,[1] Rie Irie,[3] Hirokazu Yokoyama,[4] Katsuyoshi Shimamura,[2] Shingo Usui,[1,2] Hirotoshi Ebinuma,[2] Hidetsugu Saito,[5] Chikako Watanabe,[1] Shunsuke Komoto,[1] Atsushi Kawaguchi,[1] Shigeaki Nagao,[1] Kazuo Sugiyama,[2] Ryota Hokari,[1] Takanori Kanai,[2] Soichiro Miura,[1] and Toshifumi Hibi[2]

Although nonalcoholic steatohepatitis (NASH) is associated with hypercholesterolemia, the underlying mechanisms of this association have not been clarified. We aimed to elucidate the precise role of cholesterol in the pathophysiology of NASH. C57BL/6 mice were fed a control, high-cholesterol (HC), methionine-choline-deficient (MCD), or MCD+HC diet for 12 weeks or a control, HC, high-fat (HF), or HF+HC diet for 24 weeks. Increased cholesterol intake accelerated liver fibrosis in both the mouse models without affecting the degree of hepatocellular injury or Kupffer cell activation. The major causes of the accelerated liver fibrosis involved free cholesterol (FC) accumulation in hepatic stellate cells (HSCs), which increased Toll-like receptor 4 protein (TLR4) levels through suppression of the endosomal-lysosomal degradation pathway of TLR4, and thereby sensitized the cells to transforming growth factor (TGF)β-induced activation by down-regulating the expression of bone morphogenetic protein and activin membrane-bound inhibitor. Mammalian-cell cholesterol levels are regulated by way of a feedback mechanism mediated by sterol regulatory element-binding protein 2 (SREBP2), maintaining cellular cholesterol homeostasis. Nevertheless, HSCs were sensitive to FC accumulation because the high intracellular expression ratio of SREBP cleavage-activating protein (Scap) to insulin-induced gene (Insig) disrupted the SREBP2-mediated feedback regulation of cholesterol homeostasis in these cells. HSC activation subsequently enhanced the disruption of the feedback system by Insig-1 down-regulation. In addition, the suppression of peroxisome proliferator-activated receptor γ signaling accompanying HSC activation enhanced both SREBP2 and microRNA-33a signaling. Consequently, FC accumulation in HSCs increased and further sensitized these cells to TGFβ-induced activation in a vicious cycle, leading to exaggerated liver fibrosis in NASH. *Conclusion*: These characteristic mechanisms of FC accumulation in HSCs are potential targets to treat liver fibrosis in liver diseases including NASH. (HEPATOLOGY 2014;59:154-169)

Abbreviations: ABCA1, adenosine triphosphate-binding cassette A1; ALT, alanine aminotransferase; Bambi, bone morphogenetic protein and activin membrane-bound inhibitor; CCl_4, carbon tetrachloride; CE, cholesterol ester; COPII, coat protein complex II; ER, endoplasmic reticulum; FBS, fetal bovine serum; FC, free cholesterol; HC, high cholesterol; HF, high fat; HMGCR, 3-hydroxy-3-methyl-glutaryl-CoA reductase; HSC, hepatic stellate cell; ICAM-1, intercellular adhesion molecule-1; Insig, insulin-induced gene; LDLR, low-density lipoprotein receptor; LPS, lipopolysaccharide; MβCD, methyl-β-cyclodextrin; MCD, methionine-choline deficient; mRNA, messenger RNA; NASH, nonalcoholic steatohepatitis; NPC1, Niemann-Pick C1; PCR, polymerase chain reaction; PPAR, peroxisome proliferator-activated receptor; Scap, SREBP cleavage-activating protein; siRNA, small interfering RNA; SMA, smooth muscle actin; SREBP, sterol regulatory element-binding protein; TGF, transforming growth factor; TLR4, Toll-like receptor 4; TNF, tumor necrosis factor; TUNEL, terminal deoxynucleotidyl transferase-mediated deoxyuridine nick-end labeling; VCAM-1, vascular cell adhesion molecule-1.

From the [1]Division of Gastroenterology and Hepatology, Department of Internal Medicine, National Defense Medical College, Saitama, Japan; [2]Division of Gastroenterology and Hepatology, Department of Internal Medicine, Keio University School of Medicine, Tokyo, Japan; [3]Department of Pathology, Kawasaki Municipal Hospital, Kanagawa, Japan; [4]Health Center, Keio University School of Medicine, Tokyo, Japan; [5]Graduate School of Pharmaceutical Sciences, Keio University Faculty of Pharmacy, Tokyo, Japan.

Nonalcoholic steatohepatitis (NASH) is a progressive disease that can cause cirrhosis or liver-related complications.[1] It very often accompanies lifestyle diseases including hypercholesterolemia. Several studies have shown that statins and ezetimibe (cholesterol-lowering agents) improve liver fibrosis in patients with NASH.[2] Furthermore, we have recently reported that free cholesterol (FC) accumulation in hepatic stellate cells (HSCs) plays an important role in the pathogenesis of liver fibrosis.[3] These results drew our attention to the role of cholesterol in the pathogenesis of liver fibrosis in NASH.

Cholesterol homeostasis is tightly regulated by way of a feedback system mediated by sterol regulatory element-binding protein (SREBP)2.[4,5] The low-density lipoprotein receptor (LDLR) and 3-hydroxy-3-methylglutaryl-CoA reductase (HMGCR), which play important roles in maintaining cholesterol uptake and synthesis, respectively, are predominantly regulated by SREBP2.[6] Nascent SREBP2 localizes to the endoplasmic reticulum (ER) membrane and forms tight complexes with SREBP cleavage-activating protein (Scap), a membrane-embedded escort protein.[7] When membrane cholesterol levels are low, the SREBP2-Scap complex is incorporated into the coat protein complex II (COPII)-coated vesicles.[6,8] Consequently, SREBP2 translocates to the nucleus and activates transcription of several target genes involved in the biosynthesis and uptake of cholesterol.[6] When excess cholesterol accumulates in the ER membranes, it changes Scap to an alternate conformation, allowing it to bind to resident ER proteins, insulin-induced gene (Insig)-1, and Insig-2.[9] This binding precludes the binding of COPII. Consequently, the SREBP2-Scap complex remains in the ER, transcription of the target genes declines, and cholesterol synthesis and uptake fall.[4,6]

Furthermore, recent studies have shown that the primary transcript of SREBP2 also encodes miR-33a, a microRNA that regulates cholesterol metabolism by way of factors such as adenosine triphosphate-binding cassette A1 (ABCA1) and Niemann-Pick C1 (NPC1), suggesting transcriptional regulation by *SREBF2* modulates the cellular capacity for producing not only an active transcription factor but also the expression of miR-33a.[10]

By studying two mouse models of NASH, we attempted to clarify the precise role of cholesterol in the pathophysiology of NASH. As we found that the major causes of the exacerbation of liver fibrosis in NASH involved FC accumulation in HSCs, we investigated the underlying mechanisms of FC accumulation in HSCs and its role in the pathogenesis of NASH.

Materials and Methods

Please refer to the Supporting Materials and Methods for more detailed descriptions.

Reagents. Reagents were obtained as follows: low density lipoprotein (LDL), methyl-β-cyclodextrin (MβCD)/cholesterol complex, lipopolysaccharide (LPS), chloroquine, and MG-132 were from Sigma (St. Louis, MO). 25-HC was from Wako Pure Chemical Industries (Osaka, Japan). Transforming growth factor beta (TGFβ) was from R&D Systems (Minneapolis, MN). Peroxisome proliferator-activated receptor gamma (PPARγ)-small interfering RNA (siRNA), SREBP2-siRNA, LDLR-siRNA, Scap-siRNA, Insig-1-siRNA, bone morphogenetic protein and activin membrane-bound inhibitor (Bambi)-siRNA, and control-siRNA were from Invitrogen (Carlsbad, CA). Anti-miR33a, pre-miR33a, and control-miR33a were from Ambion (Austin, TX).

Animal Studies. Nine-week-old male C57BL/6J mice (CLEA Japan, Tokyo, Japan) were fed a CE-2 (control; CLEA Japan), CE-2 with 1% cholesterol (HC), methionine-choline-deficient (MCD; Cat. No. 960439; ICN, Aurora, OH), or MCD with 1% cholesterol (MCD+HC) diet for 12 weeks. As another animal model of NASH, 9-week-old male C57BL/6J mice were also fed a CE-2, HC, high-fat (HF; prepared by CLEA Japan according to the #101447 composition of

Received September 30, 2012; accepted June 20, 2013.
Supported in part by a Grant-in-Aid for Scientific Research from the Ministry of Education, Culture, Sports, Science, and Technology of Japan (to K. Tomita)
**These authors contributed equally to this work.*
Address reprint requests to: Kengo Tomita, M.D., Division of Gastroenterology and Hepatology, Department of Internal Medicine, National Defense Medical College, 3-2 Namiki, Tokorozawa-shi, Saitama 359-8513, Japan. E-mail: kengo@ndmc.ac.jp; fax: +81 4-2996-5201.

View this article online at wileyonlinelibrary.com.
DOI 10.1002/hep.26604
Potential conflict of interest: Nothing to report.
Additional Supporting Information may be found in the online version of this article.

Dyets, Bethlehem, PA), or HF with 1% cholesterol (HF+HC) diet for 24 weeks. In the same way, 7-8-week-old C57BL/6 Toll-like receptor (TLR)4-deficient mice (Oriental BioService, Kyoto, Japan) were fed the control, HC, MCD, or MCD+HC diets for 8 weeks or the control, HC, HF, or HF+HC diets for 20 weeks. All animals received humane care in compliance with the criteria outlined in the "Guide for the Care and Use of Laboratory Animals," prepared by the US National Academy of Sciences and published by the US National Institutes of Health.

HSC Isolation and Cell Culture. Wild-type or TLR4-deficient HSCs were isolated from the livers of mice as described.[3] We cultured HSCs on uncoated 6-well plastic tissue culture dishes in serum-depleted Dulbecco's modified Eagle's medium (DMEM), DMEM containing 1% or 10% fetal bovine serum (FBS), and used them as nonpassaged primary cultures or cultures at passage 3-6.

Statistical Analysis. All data are expressed as means (standard error of the mean [SEM]). Statistical analyses were performed using the unpaired Student *t* test or one-way analysis of variance (ANOVA) ($P < 0.05$ was considered significant). When the ANOVA analyses were applied, differences in mean values among groups were examined by Fisher's multiple comparison test.

Results

Increased Cholesterol Intake Accelerates Liver Fibrosis in NASH Without Affecting the Degree of Hepatocellular Injury or Macrophage Recruitment or Activation. Compared with the livers of the MCD diet-fed mice, the livers of the MCD+HC diet-fed mice showed markedly increased centrizonal fibrosis (Supporting Fig. 1A-C). As observed in the MCD diet-induced NASH model, the extent of fibrosis was significantly enhanced in the livers of the HF+HC diet-fed mice, compared with the HF diet-fed mice (Supporting Fig. 1D-F).

HC diet feeding alone was not sufficient to cause liver fibrosis over 12 and 24 weeks (Supporting Fig. 1). In addition, increased intake of cholesterol did not significantly impact hepatocellular damage in the two mouse models of NASH (Supporting Fig. 2). There was no impact on the hepatic messenger RNA (mRNA) levels of Cyp27a1 or on the hepatic content of mitochondrial FC (Supporting Fig. 3).

Similarly, the increased cholesterol intake did not increase macrophage recruitment or activation in either of the two mouse models of NASH (Supporting Fig. 4). Neither did the increased cholesterol intake induce the formation of hepatic macrophage foam cells or cause liver inflammation in these mouse models (Supporting Figs. 1A,D, 5A). In Kupffer cells, there was also no impact on the mRNA levels of Cyp27a1 or on the cholesterol content of both the mitochondria and late endosomes/lysosomes (Supporting Fig. 5B-D). Furthermore, the increased cholesterol intake significantly exaggerated liver fibrosis in Kupffer cell-depleted mice with NASH (Supporting Fig. 6).

FC Accumulation in HSCs Is Enhanced in NASH and Up-Regulates TLR4 Protein Expression and Down-Regulates Bambi mRNA Expression in HSCs. HC, MCD, and HF diet feeding significantly increased FC levels in HSCs compared with the corresponding control diet feeding (Supporting Fig. 7A,D). Further, FC levels were significantly higher in HSCs from the MCD+HC and HF+HC diet-fed groups than in those from the other corresponding groups (Supporting Fig. 7A,D).

The mRNA expression levels of Bambi, the TGFβ pseudoreceptor, were significantly lower in HSCs from the HC, MCD, and HF diet-fed groups than in those from the corresponding control diet-fed groups and in HSCs from the MCD+HC and HF+HC diet-fed groups than in those from the other corresponding groups (Supporting Fig. 7B,E).

HC, MCD, and HF diet feeding increased the amount of TLR4 protein expressed in HSCs. In addition, HSCs from the MCD+HC and HF+HC diet-fed groups showed higher TLR4 protein expression than those from the other corresponding groups (Supporting Fig. 7C,F). No significant difference was observed in the mRNA expression levels of TLR4 among the corresponding groups (Supporting Fig. 7C,F).

HSC Activation in NASH Down-Regulates PPARγ Expression and Enhances Both SREBP2 and miR-33a Signaling; Increased Cholesterol Intake Intensifies These Effects. As noted in the whole livers, the mRNA expression levels of collagen 1α1, collagen 1α2, and α smooth muscle actin (αSMA) were significantly increased in HSCs from the MCD and HF diet-fed groups compared with the corresponding control diet-fed groups. These increases were significantly enhanced by the increased intake of cholesterol (Fig. 1A,D).

The mRNA expression levels of PPARγ1 in HSCs were significantly lower in the MCD and HF diet-fed groups than in the corresponding control diet-fed groups. In addition, these decreases were significantly

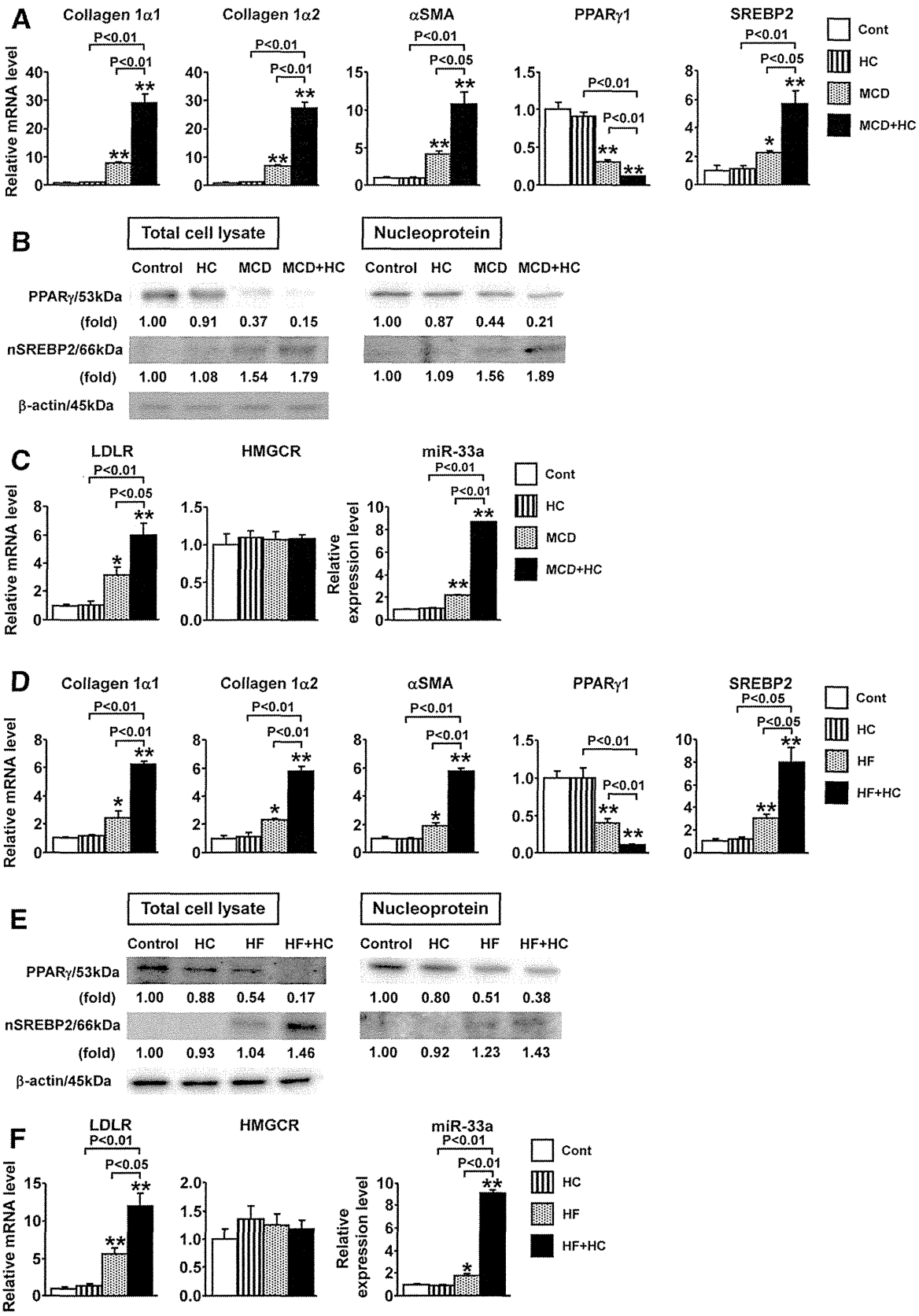

Fig. 1. Down-regulated PPARγ expression and enhanced SREBP2 and miR-33a signaling after HSC activation in the two mouse models of NASH. C57BL/6 mice (9 weeks old, male; n = 6-9/group) were fed (A-C) the control, HC, MCD, or MCD+HC diet for 12 weeks or (D-F) the control, HC, HF, or HF+HC diet for 24 weeks. (A,D) Quantification of collagen 1α1, collagen 1α2, αSMA, PPARγ1, and SREBP2 mRNA in HSCs isolated from the mice in each group. $^{**}P < 0.01$ and $^{*}P < 0.05$, compared with the control diet group. (B,E) Total and nuclear expression of PPARγ and SREBP2 protein in HSCs isolated from the mice in each group. The relative protein levels are indicated below the corresponding bands. (C,F) Quantification of LDLR and HMGCR mRNA, and miR-33a in HSCs isolated from the mice in each group. $^{**}P < 0.01$ and $^{*}P < 0.05$, compared with the control diet group. All data are expressed as means (SEM).

enhanced by the increased intake of cholesterol (Fig. 1A,D). Contrarily, the mRNA expression levels of SREBP2 were significantly higher in HSCs from the MCD and HF diet-fed groups than in those from the corresponding control diet-fed groups, and these increases were significantly enhanced by the increased intake of cholesterol (Fig. 1A,D).

The total and nuclear protein levels of PPARγ were lower in HSCs from the MCD and HF diet-fed groups than in those from the corresponding control diet-fed groups and these decreases were significantly enhanced by the increased intake of cholesterol (Fig. 1B,E). Meanwhile, the levels of the nuclear form of SREBP2 were significantly higher in HSCs from the MCD and HF diet-fed groups than in those from the corresponding control diet-fed groups. Furthermore, these increases were significantly enhanced by the increased intake of cholesterol (Fig. 1B,E).

Similar to SREBP2 expression, the expression levels of LDLR and miR-33a in HSCs were significantly higher in the MCD and HF diet-fed groups than in the corresponding control diet-fed groups. These increases were significantly enhanced by the increased intake of cholesterol (Fig. 1C,F).

In Vitro *HSC Activation Down-Regulates PPARγ Signaling, Which Enhances SREBP2 and miR-33a Signaling.* The total and nuclear forms of PPARγ were abundant in day 1 (quiescent) HSCs but declined in day 3 and 5 (activating) and day 7 (activated) HSCs (Fig. 2A). Meanwhile, the nuclear form of SREBP2 was scarce in day 1 HSCs, and its expression increased at days 3 and 5, and day 7 HSCs (Fig. 2A). Correspondingly, the PPARγ1 and SREBP2 mRNA expression levels were similar to the protein expression levels (Fig. 2A). Furthermore, the expression levels of LDLR and miR-33a in HSCs increased along with their activation (Fig. 2B).

PPARγ-siRNA treatment significantly increased the expression levels of SREBP2, LDLR, and miR-33a in quiescent HSCs (Fig. 2C). Similarly, treatment with the PPARγ antagonist significantly increased the expression levels of SREBP2, LDLR, and miR-33a in quiescent HSCs in a dose-dependent manner (Fig. 2D). On the other hand, overexpression (O/E) of PPARγ1 significantly decreased the levels of SREBP2, LDLR, and miR-33a expression in activated HSCs (Fig. 2E).

SREBP2-siRNA treatment significantly decreased the mRNA expression level of LDLR (Fig. 2F). The addition of PPARγ-siRNA did not affect the mRNA expression level of LDLR in quiescent HSCs treated with SREBP2-siRNA (Fig. 2F).

Enhancement of LDLR Expression and miR-33a Signaling Plays a Role in FC Accumulation in HSCs, Which Subsequently Increases TLR4 Protein Expression Through Suppression of the Endosomal-Lysosomal Degradation Pathway of TLR4. Suppression of LDLR mRNA expression by LDLR-siRNA treatment significantly decreased FC accumulation in HSCs treated with LDL or FBS (Fig. 3A). In HSCs treated with LDL or FBS, FC accumulation significantly decreased with the addition of anti-miR33a and increased with the addition of pre-miR33a (Fig. 3B). Furthermore, FC accumulation in HSCs increased along with their activation (Fig. 3C).

TLR4 protein expression, but not mRNA expression, in HSCs increased along with their activation (Fig. 3D). Treatment with LDL significantly increased TLR4 protein expression in HSCs and suppression of LDLR expression significantly decreased it (Fig. 3E). Similarly, the LDL-induced increase in TLR4 protein expression was significantly suppressed by the addition of anti-miR33a and significantly enhanced by the addition of pre-miR33a (Fig. 3E).

Furthermore, treatment with LDL significantly suppressed the ligand-mediated enhanced degradation of TLR4 in HSCs (Fig. 4A). Both chloroquine, an inhibitor of the endosomal-lysosomal pathways, and MG-132, an inhibitor of the proteosomal pathways, significantly increased TLR4 protein expression in HSCs (Fig. 4B). The addition of LDL did not affect the protein expression levels of TLR4 in HSCs treated with chloroquine, whereas it significantly increased the protein levels of TLR4 in HSCs treated with MG-132 (Fig. 4C,D).

FC Accumulation in HSCs Sensitizes These Cells to TGFβ-Induced Activation Through Enhancement of TLR4-Mediated Down-Regulation of Bambi. The mRNA level of Bambi significantly decreased with LPS treatment, and furthermore, the addition of LDL significantly enhanced the decrease in wild-type HSCs (Fig. 5B). A deficiency in TLR4 signaling reversed these decreases (Fig. 5B).

Wild-type HSCs, pretreated with LPS, demonstrated significant enhancement of collagen 1α1 and 1α2 mRNA expressions when stimulated with TGFβ, and showed a further increase in mRNA expression of collagen 1α1 and 1α2 when treated with LDL (Fig. 5C). A deficiency in TLR4 signaling, however, eliminated these increases (Fig. 5C).

Bambi mRNA expression did not decrease in HSCs treated with LDL, LDLR-siRNA, anti-miR33a, or pre-miR33a in the absence of LPS, but it significantly decreased when HSCs were treated with LPS

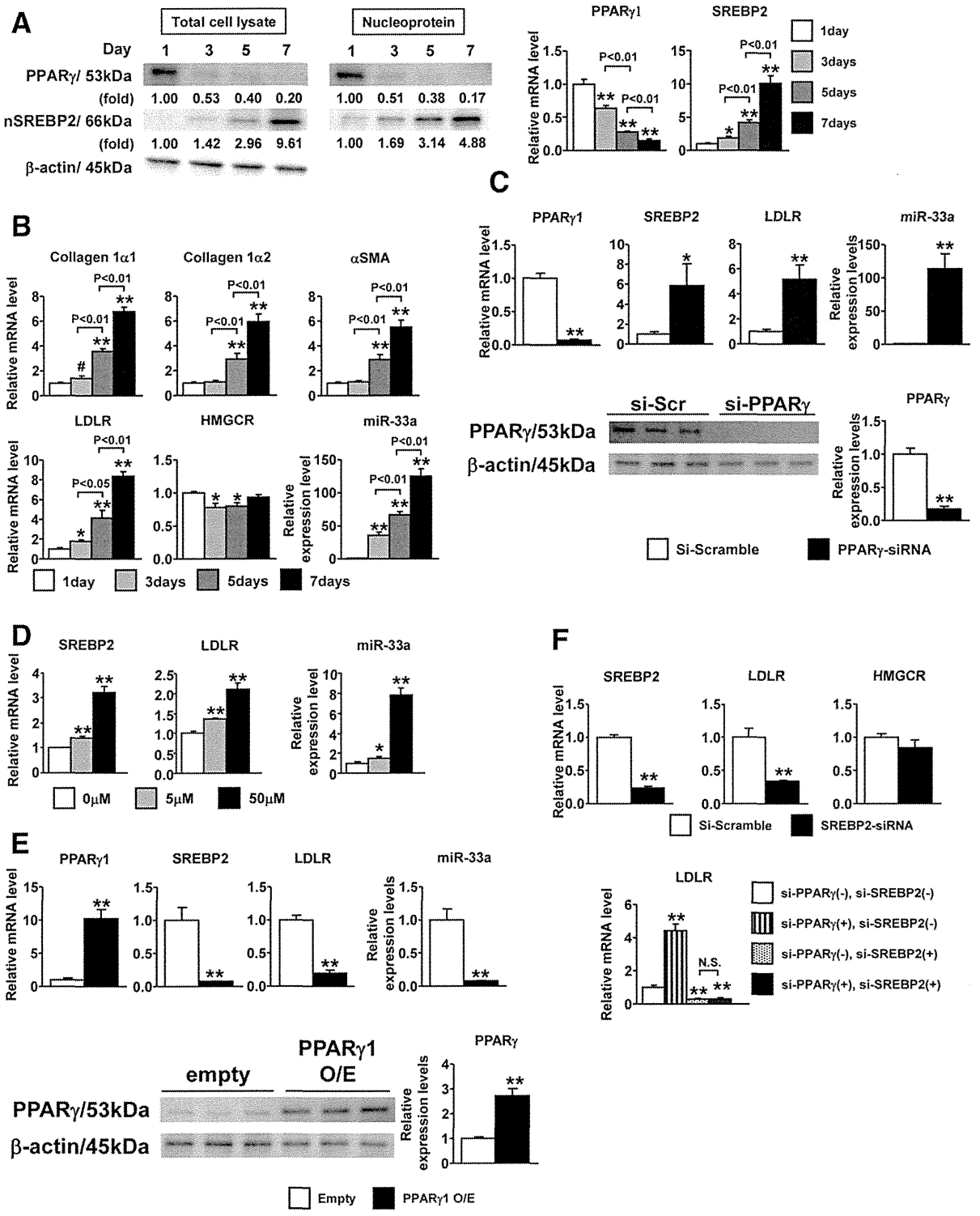

Fig. 2. Down-regulated PPARγ expression and enhanced SREBP2 and miR-33a signaling after HSC activation *in vitro*. (A) Total and nuclear protein expression (left panel) and mRNA levels (right panel) of PPARγ and SREBP2 in HSCs cultured for 1, 3, 5, or 7 days after isolation from C57BL/6 mice. The relative protein levels are indicated below the corresponding bands. $^{**}P < 0.01$, compared with the day 1 culture. (B) Quantification of collagen 1α1, collagen 1α2, αSMA, LDLR, and HMGCR mRNA and miR-33a in HSCs cultured for 1, 3, 5, or 7 days after isolation from C57BL/6 mice. Reflecting the activation of HSCs, the mRNA expression levels of collagen 1α1, collagen 1α2, and αSMA gradually increased from day 1 HSCs to day 3 and 5 HSCs to day 7 HSCs. $^{**}P < 0.01$ and $^{*}P < 0.05$, compared with the day 1 cultures. (C) Quantification of PPARγ1, SREBP2, and LDLR mRNA and miR-33a (upper panel) and PPARγ protein (lower panel) in quiescent HSCs treated with PPARγ-siRNA. $^{**}P < 0.01$ and $^{*}P < 0.05$, compared with the control culture. (D) Quantification of SREBP2 and LDLR mRNA and miR-33a in quiescent HSCs treated with the PPARγ antagonist at the indicated concentrations. $^{**}P < 0.01$ and $^{*}P < 0.05$, compared with the control culture. (E) Quantification of PPARγ1, SREBP2, and LDLR mRNA and miR-33a (upper panel), and PPARγ protein (lower panel) in activated HSCs treated with PPARγ1-O/E vector. $^{**}P < 0.01$, compared with the control culture. (F) Quantification of SREBP2, LDLR, and HMGCR mRNA in activated HSCs treated with SREBP2-siRNA (upper panel). Quantification of LDLR mRNA in quiescent HSCs treated with PPARγ-siRNA and/or SREBP2-siRNA (lower panel). $^{**}P < 0.01$, compared with the control culture. All data are expressed as means (SEM).

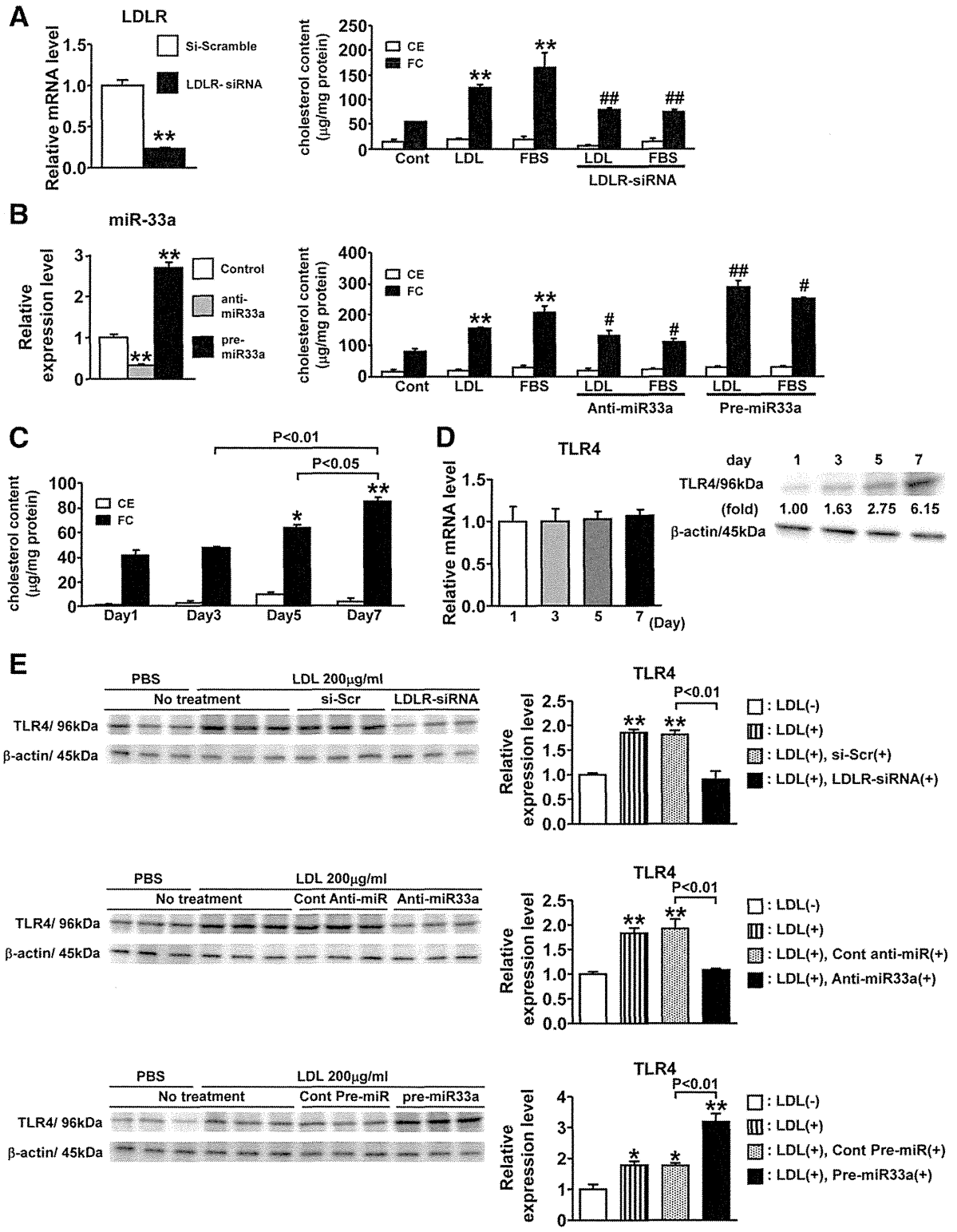

Fig. 3. FC accumulation in HSCs due to enhanced LDLR expression and miR-33a signaling. (A) Quantification of LDLR mRNA (left panel) and cellular FC and CE (right panel) in HSCs treated with LDLR-siRNA in the presence of LDL or FBS. (B) Quantification of miR-33a (left panel) and cellular FC and CE (right panel) in HSCs treated with anti-miR33a or pre-miR33a in the presence of LDL or FBS. $^{**}P < 0.01$, compared with the control culture. $^{\#\#}P < 0.01$ and $^{\#}P < 0.05$, compared with the FC contents in the corresponding cultures without the addition of LDLR-siRNA, anti-miR33a, or pre-miR33a. (C) Quantification of cellular FC and CE in HSCs cultured for 1, 3, 5, or 7 days after isolation from C57BL/6 mice. $^{**}P < 0.01$ and $^{*}P < 0.05$, compared with the day 1 cultures. (D) Quantification of TLR4 mRNA (left panel) and expression of TLR4 protein (right panel) in HSCs cultured for 1, 3, 5, or 7 days after isolation from C57BL/6 mice. The relative protein levels are indicated below the corresponding bands. (E) Expression (left panels) and quantification (right panels) of TLR4 protein in HSCs treated with control-siRNA, LDLR-siRNA, anti-miR33a, pre-miR33a, or control-miR33a in the presence of LDL. $^{**}P < 0.01$ and $^{*}P < 0.05$, compared with the control culture. All data are expressed as means (SEM).

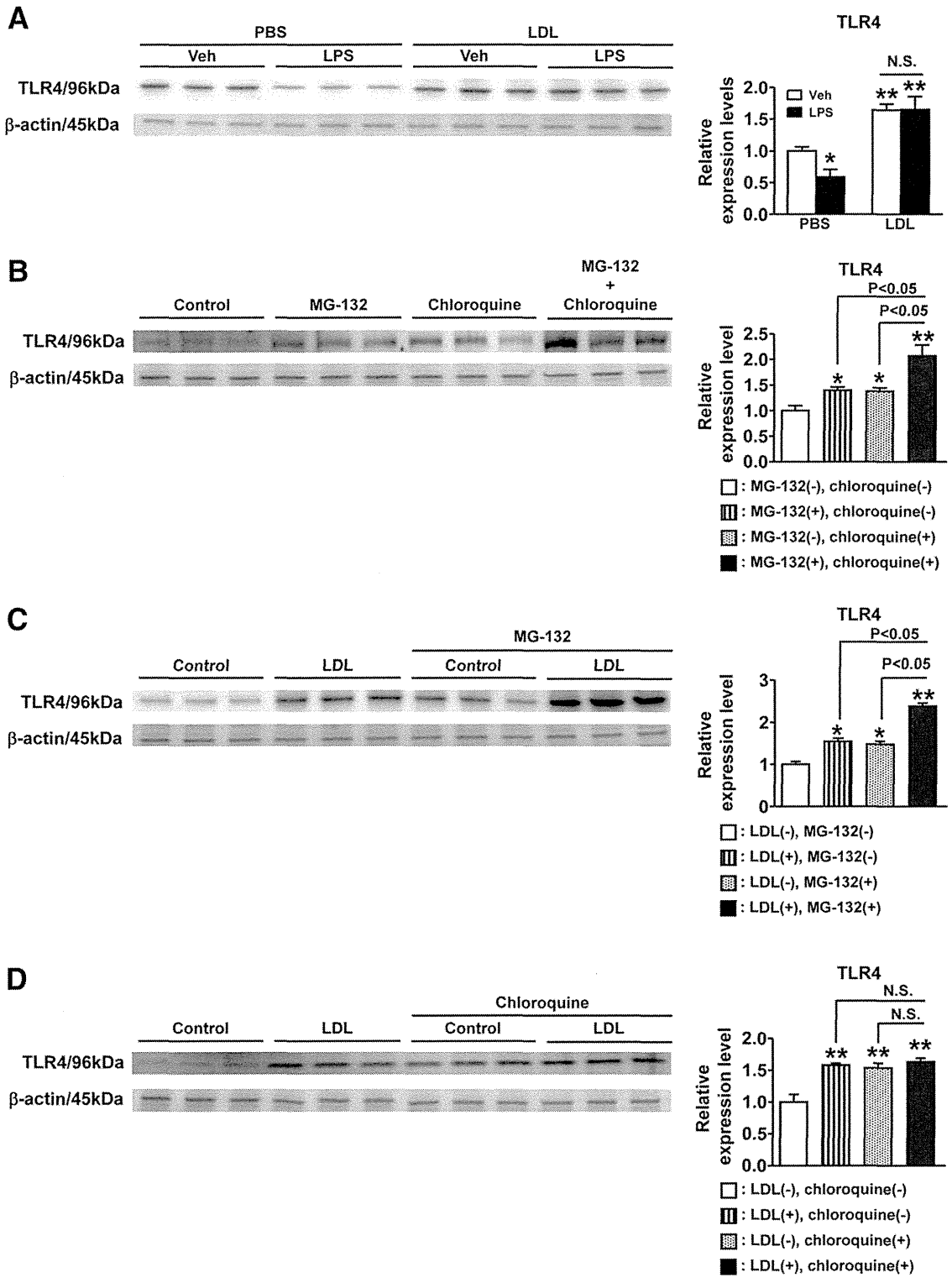

Fig. 4. FC accumulation in HSCs enhances TLR4 protein expression by suppressing the endosomal-lysosomal degradation pathway of TLR4. (A) Expression and quantification of TLR4 protein expression in vehicle-treated or LDL-treated HSCs, 60 minutes after addition of LPS (100 ng/mL), compared with cells not treated with LPS. $^{**}P < 0.01$ and $^{*}P < 0.05$, compared with the control culture, without LPS treatment. (B) Expression and quantification of TLR4 protein expression in HSCs treated with MG-132 and/or chloroquine. $^{**}P < 0.01$ and $^{*}P < 0.05$, compared with the control culture. (C) Expression and quantification of TLR4 protein expression in HSCs treated with LDL in the presence/absence of MG-132. $^{**}P < 0.01$ and $^{*}P < 0.05$, compared with the control culture. (D) Expression and quantification of TLR4 protein expression in HSCs treated with LDL in the presence/absence of chloroquine. $^{**}P < 0.01$, compared with the control culture. All data are expressed as means (SEM).

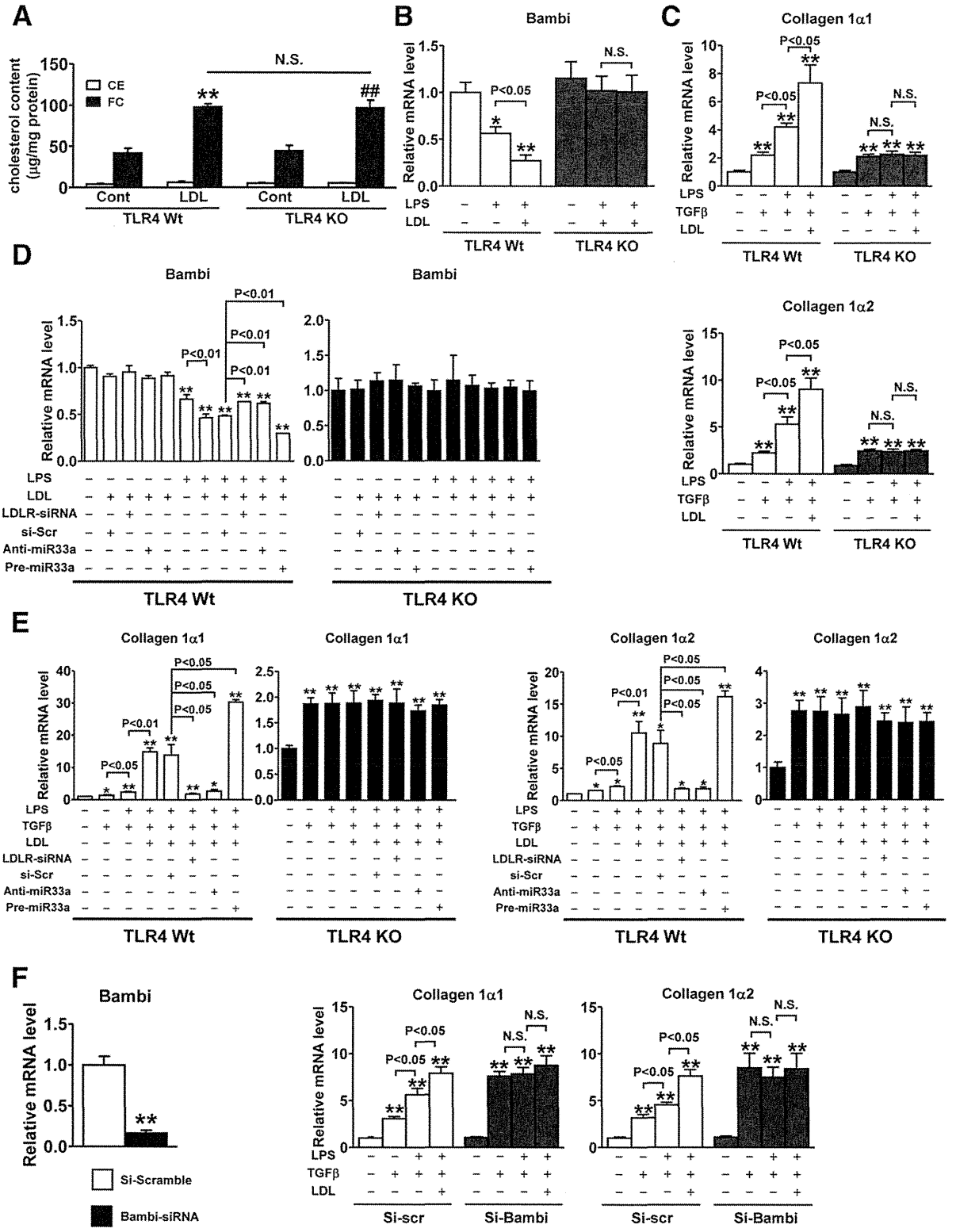

Fig. 5. FC accumulation in HSCs sensitizes HSCs to TGFβ-induced activation through enhancement of TLR4-mediated down-regulation of Bambi. (A) Quantification of cellular FC and CE in wild-type or TLR4-deficient HSCs, treated or untreated with LDL. $^{**}P < 0.01$ and $^{\#\#}P < 0.01$, compared with the corresponding control culture. (B) Quantification of Bambi mRNA in wild-type or TLR4-deficient HSCs, treated with LPS and/or LDL. $^{**}P < 0.01$ and $^{*}P < 0.05$, compared with the corresponding control culture. (C) Quantification of collagen 1α1 and collagen 1α2 mRNA in wild-type or TLR4-deficient HSCs, treated with LPS, TGFβ, and/or LDL. $^{**}P < 0.01$, compared with the corresponding control culture. (D) Quantification of Bambi mRNA in wild-type or TLR4-deficient HSCs, treated with LDLR-siRNA, control-siRNA, anti-miR33a, or pre-miR33a in the presence of LPS and/or LDL. $^{**}P < 0.01$, compared with the corresponding control culture. (E) Quantification of collagen 1α1 and collagen 1α2 mRNA in wild-type or TLR4-deficient HSCs, treated with LDLR-siRNA, control-siRNA, anti-miR33a, or pre-miR33a in the presence of LPS, TGFβ, and/or LDL. $^{**}P < 0.01$ and $^{*}P < 0.05$, compared with the corresponding control culture. (F) Quantification of Bambi mRNA in HSCs treated with Bambi-siRNA or control-siRNA (left panel). Quantification of collagen 1α1 and collagen 1α2 mRNA in wild-type HSCs, treated with Bambi-siRNA or control-siRNA in the presence of LPS, TGFβ, and/or LDL (right panel). $^{**}P < 0.01$, compared with the corresponding control culture. All data are expressed as means (SEM).

(Fig. 5D). This decrease was significantly enhanced in cells treated with LDL, whereas treatment with LDLR-siRNA reversed the LDL-induced decrease in Bambi mRNA expression (Fig. 5D). Similarly, treatment with anti-miR33a reversed the LDL-induced decrease in Bambi mRNA expression. On the other hand, treatment with pre-miR33a enhanced the LDL-induced decrease in Bambi mRNA expression (Fig. 5D). These results were in accordance with the results of FC accumulation and TLR4 protein expression in HSCs, and a deficiency in TLR4 signaling reversed all these changes (Fig. 5D).

Treatment with LDLR-siRNA reversed the LDL-induced increase in the mRNA expressions of collagen 1α1 and 1α2 in wild-type HSCs treated with LPS and TGFβ (Fig. 5E). In accordance with the results of FC accumulation and Bambi mRNA expression in HSCs, treatment with anti-miR33a reversed the LDL-induced increase in collagen 1α1 and 1α2 mRNA expression and treatment with pre-miR33a enhanced it (Fig. 5E). As is the case in Bambi mRNA expression, a deficiency in TLR4 signaling canceled all these LDL-induced changes in collagen 1α1 and 1α2 mRNA expression (Fig. 5E). In addition, treatment with Bambi-siRNA reversed the LDL-induced increase in the mRNA expression of collagen 1α1 and 1α2 in HSCs treated with LPS and TGFβ (Fig. 5F). Furthermore, in the same way as in the *in vitro* study, treatment with antagomirs against miR33a significantly alleviated the activation of HSCs in the mouse model of liver fibrosis induced by carbon tetrachloride (CCl_4). This occurred through the suppression of FC accumulation and the subsequent inhibition of TLR4-mediated down-regulation of Bambi in HSCs (Supporting Fig. 8).

Increased Intake of Cholesterol Does Not Impact Liver Fibrosis in NASH in TLR4-Deficient Mice. We used TLR4-deficient mice to assess whether the exacerbation of liver fibrosis in NASH by increased cholesterol intake was dependent on TLR4 signal transduction. Significant differences were not observed in the extent of liver fibrosis or in the hepatic mRNA levels of collagen 1α1, collagen 1α2, and αSMA, between MCD diet-fed and MCD+HC diet-fed TLR4-deficient mice (Fig. 6A-C). Similarly, the increased cholesterol intake did not enhance liver fibrosis in the HF diet-induced NASH in TLR4-deficient mice (Fig. 6D-F).

SREBP2-Mediated Feedback Regulation of Cholesterol Homeostasis Is Disrupted in HSCs and HSC Activation Further Enhances the Disruption. Nuclear accumulation of hepatic SREBP2 decreased in the two mouse models of NASH and further declined following supplementation with cholesterol (Supporting Fig. 9A). Cholesterol supplementation significantly decreased the hepatic mRNA levels of LDLR and HMGCR, which are downstream molecules of SREBP2, in both the animal models (Supporting Fig. 9B,C).

We next detailed the SREBP2-mediated feedback system of cholesterol homeostasis in hepatocytes and HSCs *in vitro*. The nuclear form of SREBP2 in hepatocytes was dramatically decreased by treatments with LDL (Fig. 7A) and 25-hydroxycholesterol, which promotes Scap-Insig complex formation.[11] These treatments also significantly decreased the nuclear form of SREBP2 in quiescent HSCs but did not affect that in activated HSCs (Fig. 7A). Quantitative analysis showed that the decrease was significantly enhanced in hepatocytes, compared with HSCs, and quiescent HSCs, compared with activated HSCs (Fig. 7A).

MβCD reportedly delivers cholesterol to cells without passing through lysosomes.[12] Treatment with a cholesterol-MβCD complex also dramatically decreased the nuclear form of SREBP2 in hepatocytes (Fig. 7A). This treatment significantly decreased the nuclear form of SREBP2 in quiescent HSCs but did not affect that in activated HSCs (Fig. 7A). Quantitative analysis showed that the decrease was significantly enhanced in hepatocytes, compared with HSCs, and in quiescent HSCs, compared with activated HSCs (Fig. 7A). Scap expression levels were much higher in quiescent and activated HSCs than in hepatocytes (Fig. 7B). However, the Insig-1 expression level in hepatocytes was comparable to that in quiescent HSCs; we did not detect any expression of Insig-1 in activated HSCs (Fig. 7B). Hepatocytes expressed Insig-2 protein, whereas we could not observe any expression of Insig-2 in HSCs (Fig. 7B).

A Scap trypsin cleavage assay[13] was subsequently performed to examine whether or not cholesterol-induced Scap conformational changes occurred in these cells. Scap, without cholesterol-induced conformational changes, yields a protected band of 27 kDa on sodium dodecyl sulfate-polyacrylamide gel electrophoresis (SDS-PAGE), whereas Scap, with the conformational change, yields a protected band of 26 kDa. Our data showed that the cholesterol-induced Scap conformational change in activated HSCs occurred to the same degree as that in quiescent HSCs or hepatocytes (Supporting Fig. 10A,B).

LDL treatment decreased the nuclear level of SREBP2 in quiescent HSCs. Treatment with Scap-siRNA or Insig-2-overexpression vector enhanced the effect, whereas treatment with Insig-1-siRNA

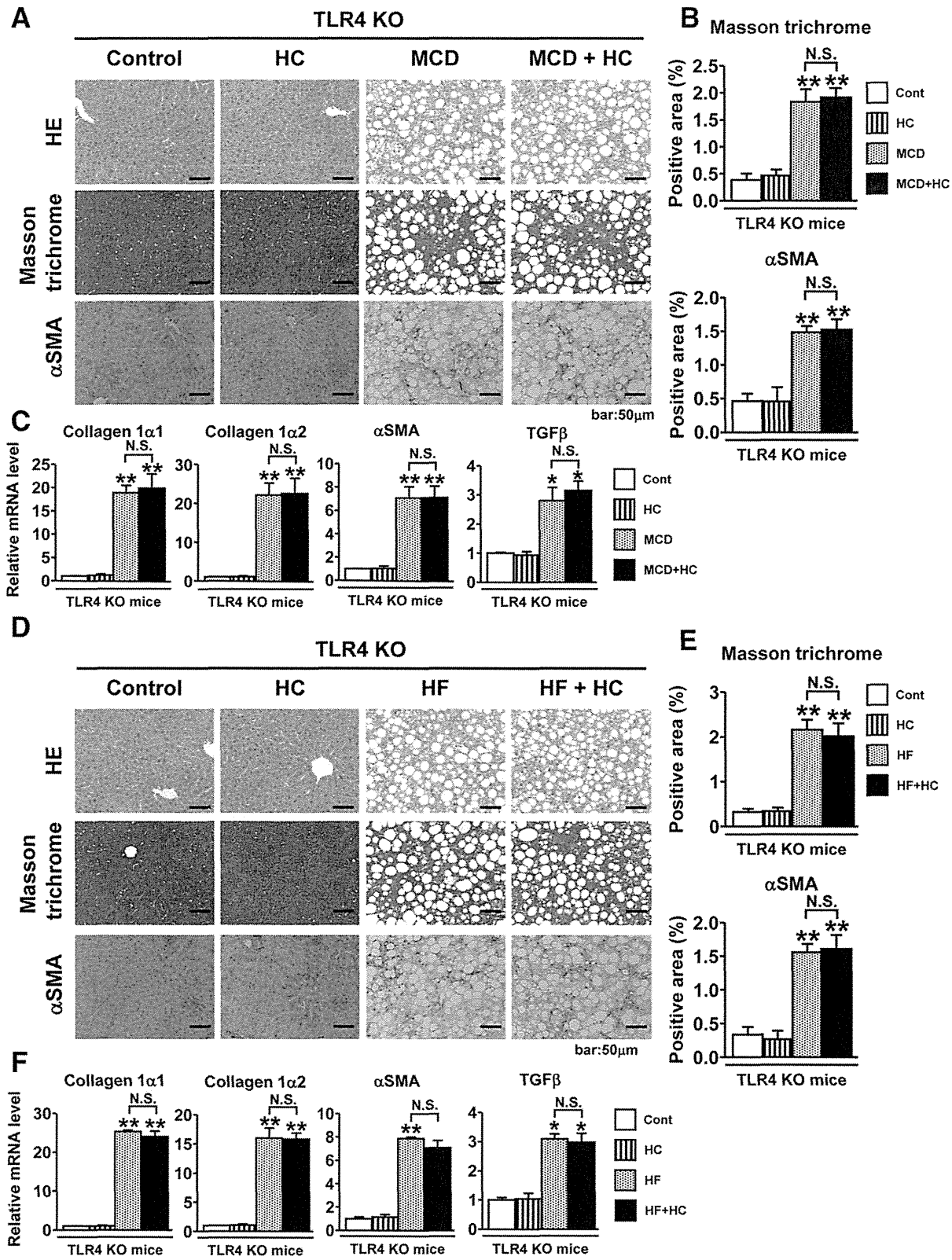

Fig. 6. Increased cholesterol intake does not impact liver fibrosis in NASH in TLR4-deficient mice. TLR4-deficient mice (7-8 weeks old; n = 4-7/group) were fed (A-C) the control, HC, MCD, or MCD+HC diet for 8 weeks or (D-F) the control, HC, HF, or HF+HC diet for 20 weeks. (A,D) Hematoxylin and eosin-stained, Masson's trichrome-stained, and αSMA-immunostained sections of representative liver samples. (B,E) Quantification of Masson's trichrome staining (upper panel) and αSMA immunostaining (lower panel). (C,F) Quantification of hepatic collagen 1α1, collagen 1α2, αSMA, and TGFβ mRNA. $^{**}P < 0.01$, compared with the control diet group. All data are expressed as means (SEM).

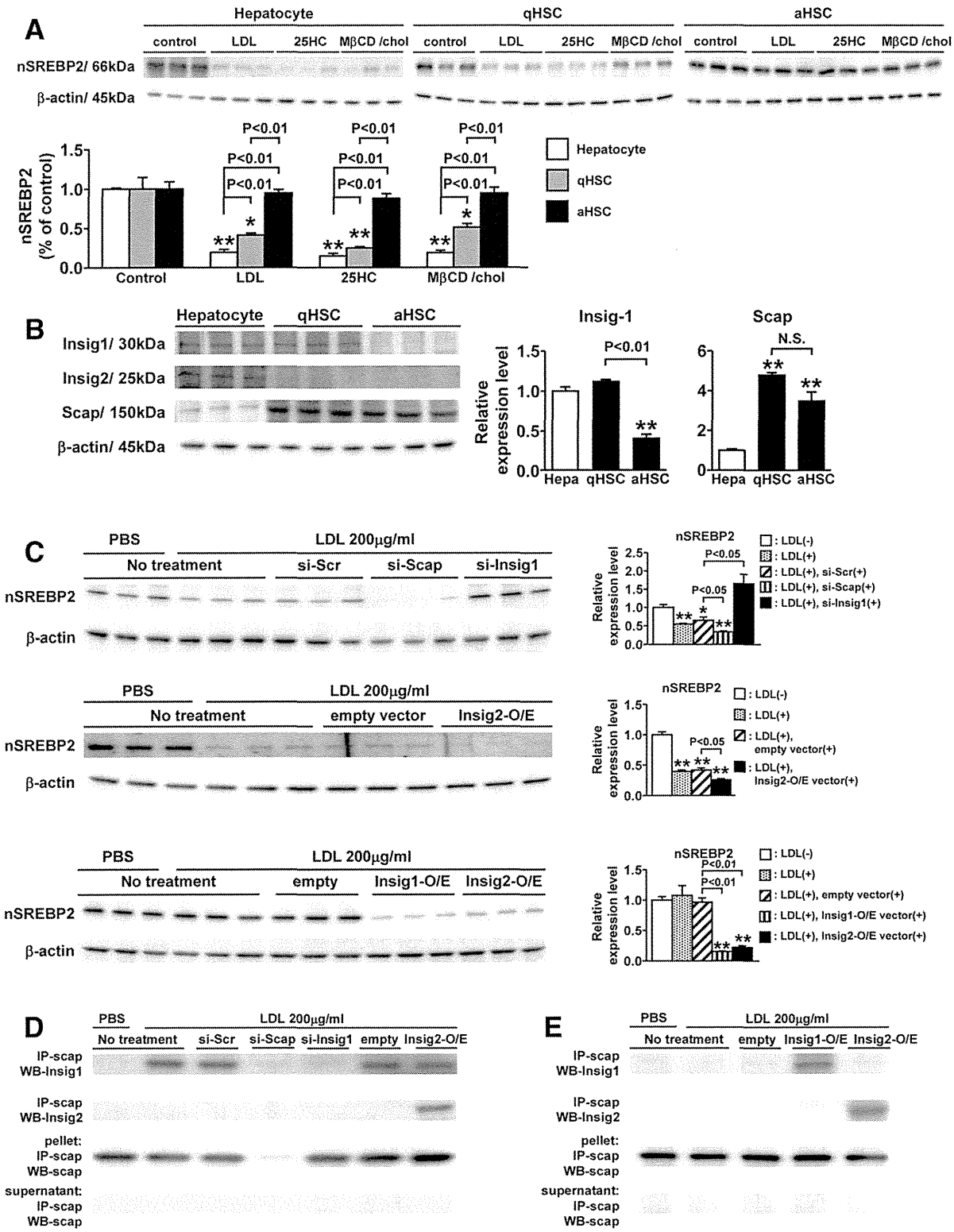

Fig. 7. The sterol regulatory systems in HSCs are disrupted and dependent on the relative amounts of Scap and Insigs. (A) Expression and quantification of the nuclear form of SREBP2 protein in hepatocytes, quiescent HSCs (qHSCs; cultured for 1 day after isolation), and activated HSCs (aHSCs; cultured for 7 days after isolation) after treatment with LDL, 25-hydroxycholesterol (25-HC), or MβCD/cholesterol complex. $^{**}P <$ 0.01 and $^{*}P < 0.05$, compared with the corresponding control culture. (B) Expression and quantification of Insig-1, Insig-2, and Scap protein in hepatocytes, qHSCs, and aHSCs. $^{**}P < 0.01$, compared with the levels in hepatocytes. (C) Expression and quantification of the nuclear form of SREBP2 protein (upper panel) in qHSCs treated with Scap-siRNA, Insig-1-siRNA, or control-siRNA in the presence/absence of LDL, (middle panel) in qHSCs treated with Insig-2-O/E vector or control vector in the presence/absence of LDL, (lower panel) in aHSCs treated with Insig-1-O/E vector, Insig-2-O/E vector, or control vector in the presence/absence of LDL. $^{**}P < 0.01$ and $^{*}P < 0.05$, compared with the control culture. (D) Immunoprecipitation analysis of Scap-Insig-1 and Scap-Insig-2 complexes in qHSCs treated with control-siRNA, Scap-siRNA, Insig-1-siRNA, control vector, or Insig-2-O/E vector in the presence of LDL. (E) Immunoprecipitation analysis of Scap-Insig-1 and Scap-Insig-2 complexes in aHSCs treated with control vector, Insig-1-O/E vector, or Insig-2-O/E vector in the presence of LDL. All data are expressed as means (SEM).

counteracted the effect (Fig. 7C, upper and middle). However, LDL treatment did not affect the nuclear level of SREBP2 in activated HSCs; overexpression of Insig-1 or Insig-2 in HSCs significantly decreased the nuclear level of SREBP2 after the addition of LDL (Fig. 7C, lower).

LDL treatment increased the level of the Scap-Insig-1 complex in quiescent HSCs, whereas cotreatment with Scap-siRNA or Insig-1-siRNA reversed this change (Fig. 7D). We could not detect any Scap-Insig-2 complex in quiescent HSCs after the addition of LDL. Overexpression of Insig-2 increased the level of the Scap-Insig-2 complex in LDL-treated quiescent HSCs (Fig. 7D). On the other hand, neither the Scap-Insig-1 nor the Scap-Insig-2 complex could be detected in activated HSCs treated with LDL or not (Fig. 7E). Overexpression of Insig-1 increased the level of the Scap-Insig-1 complex in activated HSCs treated with LDL, and similarly, overexpression of Insig-2 increased the level of the Scap-Insig-2 complex after treatment with LDL (Fig. 7E).

In addition, the feedback regulation system of cholesterol homeostasis impacted the sensitization of HSCs to TGFβ-induced activation, in a manner similar to the FC accumulation system mediated by LDLR or miR33a (Supporting Fig. 11).

HSC Activation in NASH Down-Regulates Insig-1 Expression Through the Suppression of PPARγ Signal Transduction. The Insig-1 expression level was significantly lower in HSCs from the MCD and HF diet-fed groups than in those from the corresponding control diet-fed groups (Fig. 8A,B; Supporting Fig. 12A,B). These decreases were significantly enhanced by the increased intake of cholesterol (Fig. 8A,B; Supporting Fig. 12A,B). We could not detect any difference in the Scap expression level in HSCs among the groups (Fig. 8A,B; Supporting Fig. 12A,B).

Furthermore, Insig-1 protein was abundant in quiescent HSCs but its level declined at days 3 and 5, and day 7 HSCs (Supporting Fig. 12C). We could not detect any significant difference in the Scap expression level among the groups (Supporting Fig. 12C). Similar results were obtained in terms of the mRNA expression levels of Insig-1 and Scap (Supporting Fig. 12C). Treatment with the PPARγ antagonist significantly decreased the Insig-1 expression level in quiescent HSCs in a dose-dependent manner (Fig. 8C).

Discussion

This study showed that increased cholesterol intake accelerated liver fibrosis in the two mouse models of NASH without affecting the degree of hepatocellular injury or Kupffer cell activation. The exacerbation of liver fibrosis mainly involved FC accumulation in HSCs, which increased TLR4 protein levels through suppression of the endosomal-lysosomal degradation pathway of TLR4, down-regulated the expression of the TGFβ pseudoreceptor Bambi, and thereby sensitized the cells to TGFβ-induced activation. This study also showed that FC loading of HSCs is not sufficient to induce activation but serves to enhance activation initiated by TGFβ. These results are compatible with our previous finding[3] that showed that FC accumulation in HSCs increased membrane TLR4 levels; suppressed the HSC expression of Bambi, the TLR4 target gene[14]; and subsequently exaggerated liver fibrosis in mouse models of liver fibrosis.

This study also helped to elucidate the main mechanisms by which HSCs are sensitive to FC accumulation. The SREBP2-mediated feedback system, which plays a major role in maintaining cellular cholesterol homeostasis,[5,6] was disrupted in HSCs; this disruption could be attributed to high expression of Scap and no expression of Insig-2 in these cells. This could explain why the HC diet significantly reduced SREBP2 signaling in hepatocytes but not in HSCs, and resulted in enhanced FC accumulation in HSCs.

Furthermore, HSC activation sensitized these cells to FC accumulation. Repression of PPARγ signaling underlies HSC transdifferentiation.[15] In the present study, the level of PPARγ decreased along with the activation of HSCs. The suppression of PPARγ signaling in activated HSCs decreased the cellular expression of Insig-1, which resulted in enhancing the disruption of the SREBP2-mediated cholesterol-feedback system. This could partly explain why SREBP2 signaling in HSCs was enhanced, along with their activation, although FC accumulation continued to increase.

In addition, the decreased PPARγ signaling in activated HSCs also enhanced SREBP2 expression and signaling, resulting in enhanced expression of the LDLR, the SREBP2 target gene, in HSCs. As *SREBF2* is a bifunctional locus encoding SREBP2 and miR-33a,[10] suppression of PPARγ signaling also increased the level of miR-33a in HSCs, in turn suppressing the levels of NPC1 and ABCA1 (data not shown), which are negatively regulated by miR-33a.[10] These results showed that HSC activation enhanced FC accumulation, in part because of the increased LDLR level and the decreased NPC1 and ABCA1 levels.

The present results suggest that these characteristic mechanisms in HSCs could sensitize the cells to enhanced FC accumulation after increased intake of

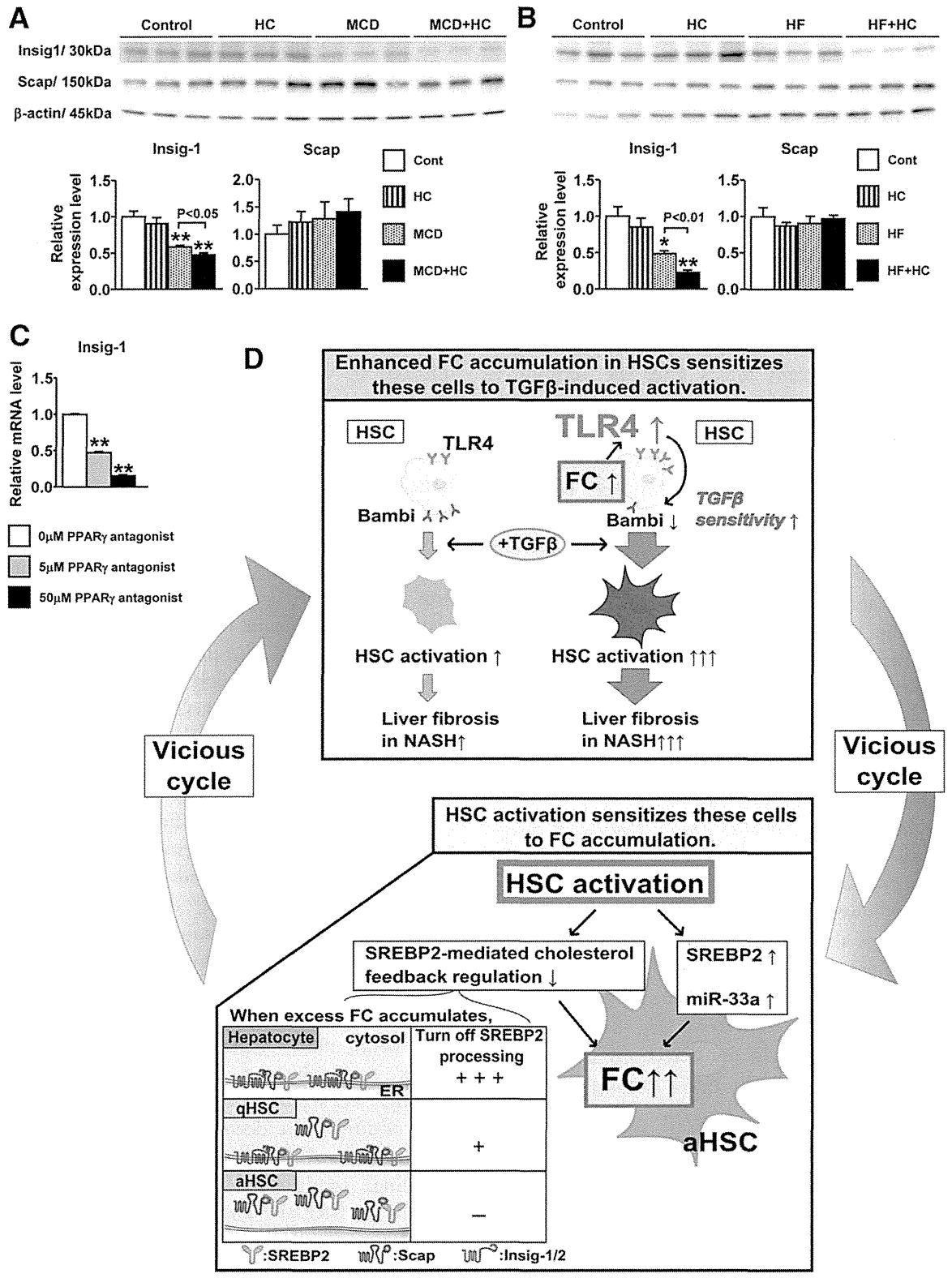

Fig. 8. Down-regulation of Insig-1 expression by HSC activation through the suppression of PPARγ signal transduction. C57BL/6 mice (9 weeks old, male; n = 6-9/group) were fed (A) the control, HC, MCD, or MCD+HC diet for 12 weeks or (B) the control, HC, HF, or HF+HC diet for 24 weeks. (A,B) Expression and quantification of Insig-1 and Scap protein in HSCs isolated from the mice in each group. $^{**}P < 0.01$ and $^{*}P < 0.05$, compared with the control diet group. (C) Quantification of Insig-1 mRNA in quiescent HSCs treated with the PPARγ antagonist. $^{**}P < 0.01$, compared with the control culture. All data are expressed as means (SEM). (D) Schematic of the characteristic mechanisms of FC accumulation in HSCs during the development of liver fibrosis in NASH. FC loading of HSCs is not sufficient to induce activation but serves to enhance activation initiated by TGFβ. Enhanced FC accumulation in HSCs plays an important role in the progression of liver fibrosis in NASH by promoting TLR4 signal transduction through suppression of the endosomal-lysosomal degradation pathway of TLR4, down-regulating the Bambi expression level, and subsequently sensitizing HSCs to TGFβ-induced activation. HSCs are sensitive to FC accumulation because of the high intracellular Scap-to-Insig expression ratio, and furthermore, HSC activation dysregulates their cholesterol metabolism, resulting in further FC accumulation and exaggerating liver fibrosis in a vicious cycle.

cholesterol and/or activation of HSCs. They also suggest that such accumulation could play an important role as a mediator of the vicious cycle of HSC activation in NASH (Fig. 8D).

There are two major pathways for cell surface receptor degradation after ubiquitination: a ubiquitin-proteasome pathway and a lysosomal degradation pathway.[16] Our present results showed that FC accumulation in HSCs inhibited the degradation of TLR4, mainly by down-regulating a lysosomal degradation pathway, which resulted in increased levels of TLR4 protein. These results are compatible with our previous report[3] showing that FC accumulation in HSCs could be involved in endosomal-lysosomal dysfunction.

The MCD diet-induced mouse model is commonly used as a model of NASH, and the resulting characteristic pathology of steatosis, mixed cell inflammatory infiltrate, hepatocellular necrosis, and pericellular fibrosis mimics that found in humans with NASH.[17,18] Nevertheless, the mice do not develop the accompanying metabolic syndrome that is often associated with human NASH. Therefore, we also used an HF diet-induced model of NASH to examine the precise role of cholesterol in the pathophysiology of NASH. As the results were similar in both mouse models of NASH, our findings may indicate a role for cholesterol in the pathophysiology of NASH.

Mari et al.[19] reported that mitochondrial FC loading accounted for hepatocellular sensitivity to TNFα. Furthermore, they showed that the mitochondrial FC content in mouse hepatocytes increased transiently only during the first 6 days of HC feeding, and thereafter returned to its prior level.[19] Our results also showed that chronic HC feeding did not significantly increase mitochondrial FC accumulation in hepatocytes. This could be one reason why an increased intake of cholesterol did not impact the hepatocellular damage in our two mouse models of NASH.

A recent report showed that accumulation of cholesterol in the lysosomes of Kupffer cells increased hepatic inflammation in the mouse model of NAFLD.[20] 27-Hydroxycholesterol is enzymatically generated from mitochondrial cholesterol by the mitochondrial P450 enzyme, Cyp27a1.[21] Further, it mobilizes cholesterol from the lysosomes to the cytoplasm, resulting in a reduction in the accumulation of lysosomal cholesterol in Kupffer cells.[20] In both mouse models of NASH, an increased intake of cholesterol did not affect the lysosomal cholesterol levels in Kupffer cells, nor did it impact the mitochondrial cholesterol levels or Cyp27a1 expression levels in Kupffer cells. These could be some reasons why increased cholesterol intake did not accelerate Kupffer cell activation in our mouse models of NASH.

In conclusion, FC accumulation in HSCs was enhanced mainly by two mechanisms: enhancement of both SREBP2 and miR-33a signaling through the suppression of PPARγ signaling along with HSC activation and disruption of the SREBP2-mediated cholesterol-feedback system in HSCs, which was characterized by a high Scap-to-Insig ratio and exaggerated by the down-regulation of Insig-1 through the suppression of PPARγ signaling along with HSC activation. Enhanced FC accumulation in HSCs plays an important role in the progression of liver fibrosis in NASH by promoting TLR4 signal transduction through suppression of the endosomal-lysosomal degradation pathway of TLR4, and subsequently sensitizing HSCs to TGFβ-induced activation. HSC activation dysregulates their cholesterol metabolism, resulting in further FC accumulation and exaggerating liver fibrosis in a vicious cycle (Fig. 8D). We believe that the characteristic mechanisms of FC accumulation in HSCs should be further studied as potential targets to treat liver fibrosis in liver diseases including NASH.

Acknowledgment: The authors thank Mina Kitazume and Miho Takabe (Keio University) for helpful advice and technical assistance, and Drs. Ikuo Inoue and Makoto Seo (Saitama Medical School) for helpful discussion and critical comments.

References

1. Schattenberg JM, Schuppan D. Nonalcoholic steatohepatitis: the therapeutic challenge of a global epidemic. Curr Opin Lipidol 2011;22:479-488.
2. Musso G, Cassader M, Gambino R. Cholesterol-lowering therapy for the treatment of nonalcoholic fatty liver disease: an update. Curr Opin Lipidol 2011;22:489-496.
3. Teratani T, Tomita K, Suzuki T, Oshikawa T, Yokoyama H, Shimamura K, et al. A high-cholesterol diet exacerbates liver fibrosis in mice via accumulation of free cholesterol in hepatic stellate cells. Gastroenterology 2012;142:152-164 e110.
4. Bengoechea-Alonso MT, Ericsson J. SREBP in signal transduction: cholesterol metabolism and beyond. Curr Opin Cell Biol 2007;19:215-222.
5. Radhakrishnan A, Goldstein JL, McDonald JG, Brown MS. Switch-like control of SREBP-2 transport triggered by small changes in ER cholesterol: a delicate balance. Cell Metab 2008;8:512-521.
6. Horton JD, Shah NA, Warrington JA, Anderson NN, Park SW, Brown MS, et al. Combined analysis of oligonucleotide microarray data from transgenic and knockout mice identifies direct SREBP target genes. Proc Natl Acad Sci U S A 2003;100:12027-12032.
7. Brown MS, Goldstein JL. A proteolytic pathway that controls the cholesterol content of membranes, cells, and blood. Proc Natl Acad Sci U S A 1999;96:11041-11048.
8. Nohturfft A, Brown MS, Goldstein JL. Sterols regulate processing of carbohydrate chains of wild-type SREBP cleavage-activating protein (SCAP), but not sterol-resistant mutants Y298C or D443N. Proc Natl Acad Sci U S A 1998;95:12848-12853.

9. Radhakrishnan A, Sun LP, Kwon HJ, Brown MS, Goldstein JL. Direct binding of cholesterol to the purified membrane region of SCAP: mechanism for a sterol-sensing domain. Mol Cell 2004;15:259-268.
10. Bommer GT, MacDougald OA. Regulation of lipid homeostasis by the bifunctional SREBF2-miR33a locus. Cell Metab 2011;13:241-247.
11. Adams CM, Reitz J, De Brabander JK, Feramisco JD, Li L, Brown MS, et al. Cholesterol and 25-hydroxycholesterol inhibit activation of SREBPs by different mechanisms, both involving SCAP and Insigs. J Biol Chem 2004;279:52772-52780.
12. Abi-Mosleh L, Infante RE, Radhakrishnan A, Goldstein JL, Brown MS. Cyclodextrin overcomes deficient lysosome-to-endoplasmic reticulum transport of cholesterol in Niemann-Pick type C cells. Proc Natl Acad Sci U S A 2009;106:19316-19321.
13. Brown AJ, Sun L, Feramisco JD, Brown MS, Goldstein JL. Cholesterol addition to ER membranes alters conformation of SCAP, the SREBP escort protein that regulates cholesterol metabolism. Mol Cell 2002;10: 237-245.
14. Seki E, De Minicis S, Osterreicher CH, Kluwe J, Osawa Y, Brenner DA, et al. TLR4 enhances TGF-beta signaling and hepatic fibrosis. Nat Med 2007;13:1324-1332.
15. Tsukamoto H, Zhu NL, Asahina K, Mann DA, Mann J. Epigenetic cell fate regulation of hepatic stellate cells. Hepatol Res 2011;41:675-682.
16. Chuang TH, Ulevitch RJ. Triad3A, an E3 ubiquitin-protein ligase regulating Toll-like receptors. Nat Immunol 2004;5:495-502.
17. Tomita K, Tamiya G, Ando S, Ohsumi K, Chiyo T, Mizutani A, et al. Tumour necrosis factor alpha signalling through activation of Kupffer cells plays an essential role in liver fibrosis of non-alcoholic steatohepatitis in mice. Gut 2006;55:415-424.
18. Leclercq IA, Farrell GC, Field J, Bell DR, Gonzalez FJ, Robertson GR. CYP2E1 and CYP4A as microsomal catalysts of lipid peroxides in murine nonalcoholic steatohepatitis. J Clin Invest 2000;105:1067-1075.
19. Mari M, Caballero F, Colell A, Morales A, Caballeria J, Fernandez A, et al. Mitochondrial free cholesterol loading sensitizes to TNF- and Fas-mediated steatohepatitis. Cell Metab 2006;4:185-198.
20. Bieghs V, Hendrikx T, van Gorp PJ, Verheyen F, Guichot YD, Walenbergh SM, et al. The cholesterol derivative 27-hydroxycholesterol reduces steatohepatitis in mice. Gastroenterology 2013;144:167-178 e161.
21. Umetani M, Shaul PW. 27-Hydroxycholesterol: the first identified endogenous SERM. Trends Endocrinol Metab 2011;22:130-135.